Coal Extraction and Utilization Research Center

Southern Illinois University at Carbondale

Thermal Healing of Defects in Oxide Scales on Iron-Chromium Alloys

J. H. Swisher, W. D. Cho, and W. W. Qiu

FINAL REPORT
January 1, 1989–August 31, 1990

Southern Illinois University at Carbondale
Carbondale, Illinois 62901

Submitted to:
U.S. Department of Energy

Contract No. DE-FC22-89PC89904

U.S. Patent clearance is not required prior to the publication of this document.

Thermal Healing of Defects in Oxide Scales on Iron-Chromium Alloys

DOE/PC/89904--T13

DE90 011453

by

J. H. Swisher, W. D. Cho, and W. W. Qiu
Department of Mechanical Engineering and Energy Processes
Southern Illinois University at Carbondale
Carbondale, Illinois 62901

Final Report
January 1, 1989–August 31, 1990

Submitted to
U.S. Department of Energy
Contract Number DE-FC22-89PC89904

April 1990

DISCLAIMER

Thermal Healing of Defects in Oxide Scales on Iron-Chromium Alloys

J. H. Swisher, W. D. Cho, and W. W. Qiu
Department of Mechanical Engineering and Energy Processes
Southern Illinois University at Carbondale
Carbondale, IL 62901

ABSTRACT

An investigation completed earlier on the thermal healing of defects in Wustite scales on iron was extended to study the same phenomena in several Fe-Cr alloys. Included were a series of commercial Fe-Cr-Mo alloys containing up to 9% Cr, the 9% Cr alloy electroplated with Cr, and an Fe-25Cr-6Al alloy. Three types of experiments were conducted to study lateral mass transport of oxide into flaws introduced to simulate damage to protective oxide layers caused by particle erosion. It was found that flaw healing by lateral mass transport in the alloys was much slower than in unalloyed iron, which is understandable because elements like Cr and Al improve general oxidation resistance by facilitating the formation of scales with low diffusion rates. Experiments with electroplated Cr coatings showed potentially beneficial effects with respect to both general oxidation and flaw healing behavior. Compared to unplated material, the oxidation rate was lower, and the FeO outer scale was more adherent. Also the Cr content of the oxide in healed flaws was higher than in the oxide adjacent to the flaws.

INTRODUCTION

In many fields of engineering and science, the size and sophistication of the body of published literature parallels its practical importance. The general oxidation of metals and alloys is a good example. Three of many books on the subject were published by Hauffe(1), Douglass(2), and Birks and Meier (3). Recent books on oxidation and other types of hot gas corrosion in coal combustion and coal conversion environments have been published by Meadowcroft and Manning(4), Norton(5) and Rothman(6). Since iron-chromium alloys have good resistance to thermal oxidation, their properties are discussed extensively in the books listed above. For the research to be described here, a relevant series of articles was published in a symposium book on corrosion of steels in CO_2(7-9). Depending on alloy composition and exposure conditions, the oxide phases formed may be Cr_2O_3, Fe-Cr spinels, iron oxides with dissolved chromium, and duplex scales containing two or more phases.

Only one article published prior to 1989 was found that discussed the healing of flaws in protective oxide scales on alloys. Schutz(10) studied the formation and healing of flaws in high chromium alloy steels during thermal cycling. He found there to be a critical strain rate below which healing occurs by the formation of new oxide in the cracks. In 1989, a symposium was held which emphasized the combined effects of corrosion and erosion(11). An article in this book by Swisher, Cho, and Chang(12) examined the thermal healing of defects in FeO on unalloyed iron. This research was a precursor to the work described here. It was found that lateral diffusion in FeO scales occurred sufficiently fast to contribute to the smoothing of scratches or grooves cut into the scale. These defects were designed to simulate damage to the oxide caused by abrasive particles. The results discussed in Ref. 12 are extended in the present study to examine the same effects in iron-chromium alloys.

EXPERIMENTAL

The compositions of the alloys used as specimen materials are listed in Table 1. Alloys in the Fe-Cr-Mo series are commonly used in boiler tubes and oil refinery plants, and are commercially available. Specimens of most of these alloys were procured from Metal Samples Co., Inc., Munford, Alabama. Grade 304 stainless steel is, of course, widely used at both ambient and elevated temperatures. The Fe-25Cr series of alloys was provided by Battelle-Columbus Laboratories, one of several U.S. Department of Energy contractors evaluating the alloys for fossil energy applications.

In addition, some specimens of the 9Cr-1Mo alloy were electroplated with chromium to a thickness of 25 micrometers (0.001 in). It was found that the platings had to be diffusion bonded to the steel to resist spalling during oxidation. Diffusion bonding was carried out at 900°C in an H_2 atmosphere for times ranging from 4 to 18 hours.

An attempt was made to preoxidize specimens for defect healing experiments under conditions which duplicated the procedure and results of a prior investigator(8). Unfortunately, the scales formed under such conditions were either too thin for defect healing experiments or were non-adherent. Therefore a task was added to study general oxidation of the alloys of interest

Table 1 Experimental Alloy Compositions

Alloy Designation	w/o Cr	w/o Mo	w/o Ni	w/o Al	Other elements
2 1/4 Cr-½Mo steel	2.3	0.6			0.1 C, 0.5 Mn, 0.2 Si
5 Cr-½Mo steel	4.4	0.5	0.2	----	0.1 C, 0.5 Mn, 0.3 Si, 0.1 Cu
7 Cr-½Mo steel	6.9	0.6	0.3	----	0.1 C, 0.4 Mn, 0.6 Si
9 Cr-1 Mo steel	8.3	1.0	0.1	----	0.1 C, 0.5 Mn, 0.6 Si, 0.1 Cu
304 Stainless	18	----	8	----	0.1 C, 2.0 Mn, 1.0 Si
Fe-25 Cr	25.0	----	<0.01	<0.01	0.001 C, <0.01 Mn, <0.01 Si
Fe-25 Cr-6 Al	24.6	----	<0.01	5.9	0.004 C, <0.01 Mn, <0.01 Si
Fe-25 Cr-20 Ni	24.8	----	19.9	0.01	0.004 C, <0.01 Mn, <0.01 Si

under conditions which produced the type of oxide scale desired. These experiments were carried out in a Lindberg controlled-atmosphere tube furnace in CO-CO_2 gas mixtures and in air in the temperature range from 900 to 1150°C. This temperature range is above the application limits for the Fe-Cr-Mo alloys, so the results are useful mainly for characterizing the phenomena of interest here.

From the general oxidation data, it was decided to use the following conditions to preoxidize specimens for defect healing experiments: for the Cr-Mo steels, specimens were reacted for 16 hours at 1150°C with $CO/CO_2 = 1.76$ in the gas atmosphere; for some of the Fe-25 Cr-6Al experiments, specimens were reacted for 48 hours at 1150°C in air.

Three types of defect healing experiments were conducted. In one type, preoxidized specimens containing scribed defects were reheated in evacuated and sealed Vycor capsules. In a second type, similar specimens were reexposed to the same gas atmosphere as that used for preoxidation. In both of these types of healing experiments, defects were normally cut through the scales with a wire saw. The wire used was 0.25 mm dia. and contained diamond dust incorporated into a steel matrix. On occasions when the scale was less than 10 micrometers in thickness, a diamond scriber was used instead of the wire saw. In the third type, platinum bands were diffusion-bonded into grooves in the alloy to simulate bare metal at the base of a flaw. The lateral growth of oxide over the platinum bands was then studied by heating the specimens in an oxidizing atmosphere. The procedures used for defect healing will be discussed further in the Results and Discussion section.

For the general oxidation experiments, the conversion of metal to oxide or metal wastage was measured by mechanical and chemical removal of the scale. For the latter, Clarke's solution was used for the Cr-Mo steels, and hot nitric acid for the higher chromium alloys. The weight loss of the specimen after removal of the scale was the basis for the metal wastage determination.

The oxides formed during both general oxidation and defect healing treatments were characterized using x-ray diffraction, optical microscopy, scanning electron microscopy (SEM), energy dispersive x-ray measurements (EDX), and Auger electron spectroscopy (AES).

RESULTS AND DISCUSSION

Characterization of Cr-plated specimens: Photomicrographs of cross-sections of Cr-plated specimens as-received and after diffusion bonding for 18 hr at 900°C are shown in Figure 1. The original coating was quite uniform and approximately 25 micrometers thick. After diffusion bonding, there was no resolvable difference in structure between the surface and near-surface regions. The Cr concentration at the surface, however, was easily measured by energy dispersive x-ray analysis (EDX). Data relating the surface concentration of Cr to diffusion bonding time are shown in Figure 2. After a bonding time of 18 hr, the Cr concentration is nearly twice the bulk composition of 8.3%; and after 4 hr, the concentration is close to that of type 304 stainless steel.

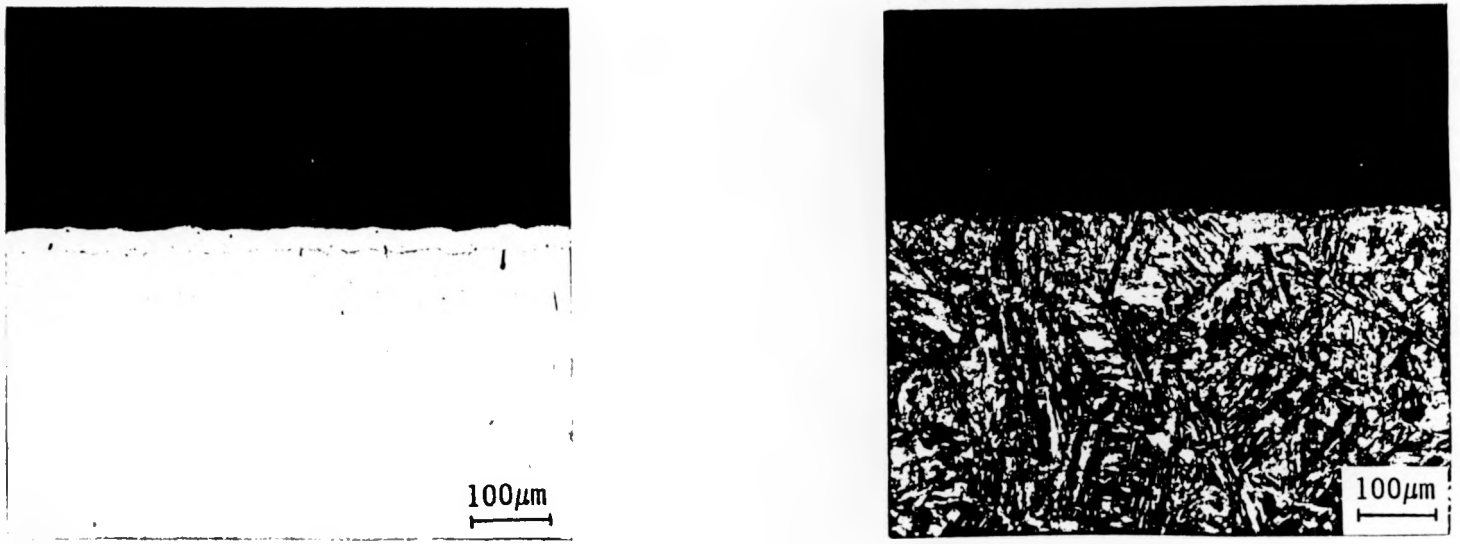

(a) (b)

Figure 1. (a) Cross section of as-received, Cr-plated 9Cr-1Mo Steel specimen (unetched) (b) Same specimen after diffusion bonding in H_2 at 900°C for 18 hours (etched with Nital).

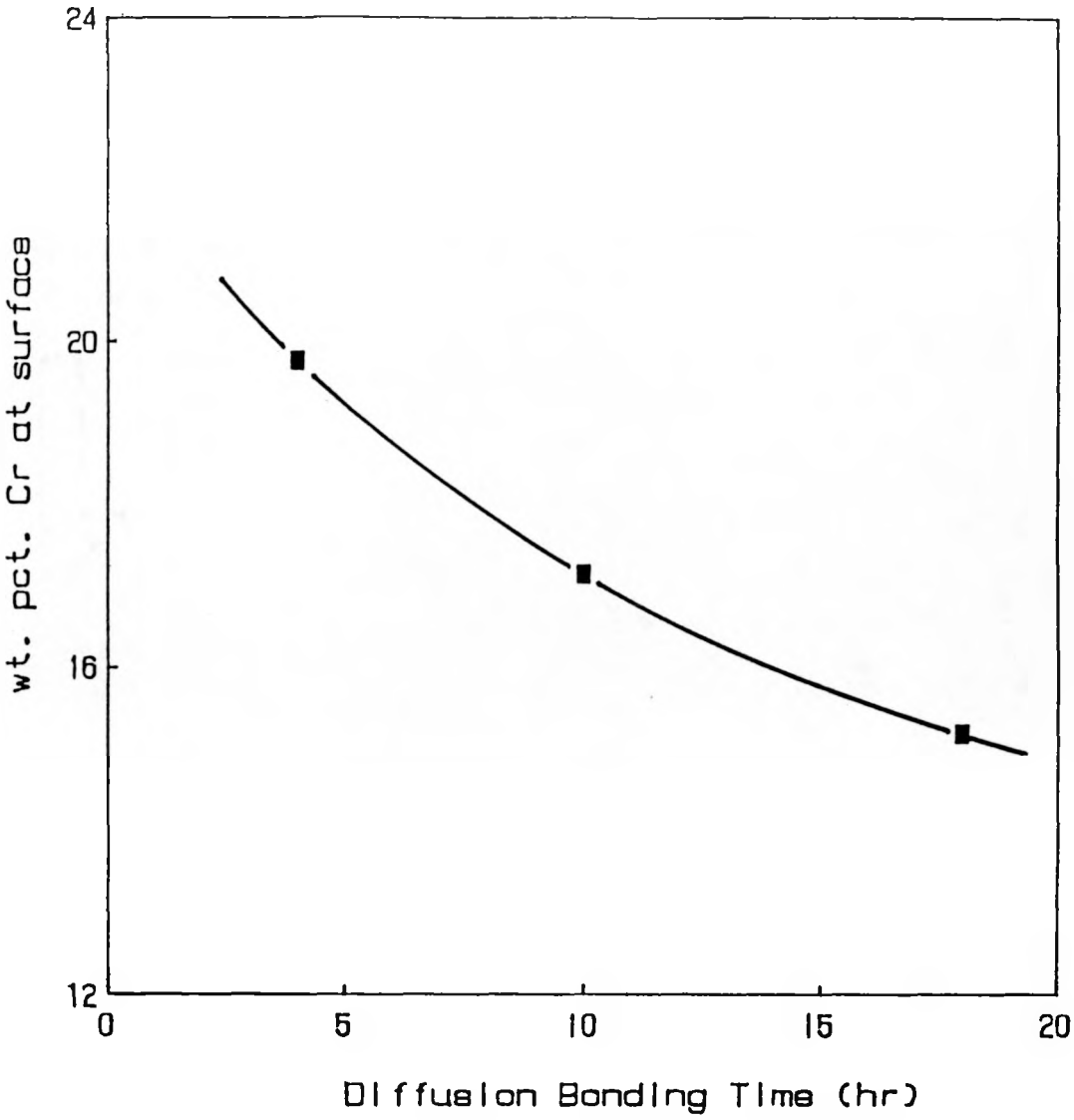

Figure 2. Chromium surface concentration as a function of diffusion bonding time at 900°C in H_2 for Cr-plated, 9Cr-1Mo alloy.

An analysis was carried out to compare the results shown in Figure 2 with the results of an approximate diffusion calculation. For the diffusion of solute originally in a thin film on the surface into the bulk of a thick specimen, an equation given by Crank (13) can be modified slightly for the conditions of the experiment to give

$$C - Co = \frac{hd}{\sqrt{\pi Dt}} \exp\left(-\frac{x^2}{4Dt}\right)$$

where C is the concentration of Cr at any time and location (g/cm^3)
Co is the initial Cr concentration in the alloy (0.647 g/cm^3)
h is the plating thickness (cm)
d is the density of the alloy (7.8 g/cm^3)
D is the diffusion coefficient (cm^2/s)
t is the time in seconds
and x is the distance from the surface (cm)

Since only surface concentrations were measured by EDX, x=0 and

$$D = \frac{h^2 d^2}{\pi t (C - Co)^2}$$

This equation gives only an approximate value because there is an ambiguity in defining x with a plating thickness as large as 25 micrometers.

Substituting values for a reaction time of 18 hr yields a value of 6×10^{-9} cm^2/s for the diffusion coefficient of Cr. Reference book data (14) yield a value of 1.3×10^{-9} cm^2/s for diffusion of Cr in an Fe-11.8% Cr alloy at the same temperature. The agreement is considered reasonably good if one considers that the 9 Cr alloy also contains Mo, C, Mn, Si, and Cu at percentages in the range from 0.1 to 1.0.

General oxidation behavior: The first set of experiments on general oxidation consisted of examining the time dependence of the extent of oxidation of the 9 Cr-1 Mo alloy. The results, shown in Figure 3, demonstrate that oxidation follows a linear rate law between 10 and 37 hours of reaction time at 1150°C. As will be discussed later, the scale consisted of a relatively thick layer of loosely adherent FeO over a thin layer of an Fe-Cr spinel. Since the scale did not serve as an effective diffusion barrier to oxidation, linear rather than parabolic oxidation kinetics is not surprising. There is also a possibility that slow dissociation of CO_2 on the surface of the specimen was a factor in making the oxidation rate linear with time (15). Note that the extent of oxidation for the Cr-plated specimen was less than for an unplated specimen at the same reaction time. This effect would probably be more dramatic at lower temperatures because, at 1150°C, Cr diffuses rather rapidly from the near-surface region, thus reducing the beneficial effect on oxidation resistance.

General oxidation results are presented in Figure 4 for unalloyed iron and the series of Fe-Cr-Mo alloys. The metal wastage rate is plotted vs %Cr in the alloys for various temperatures, a gas composition of $CO/CO_2 = 0.59$, and a reaction time of 48 hours. As one would expect, the metal wastage rate

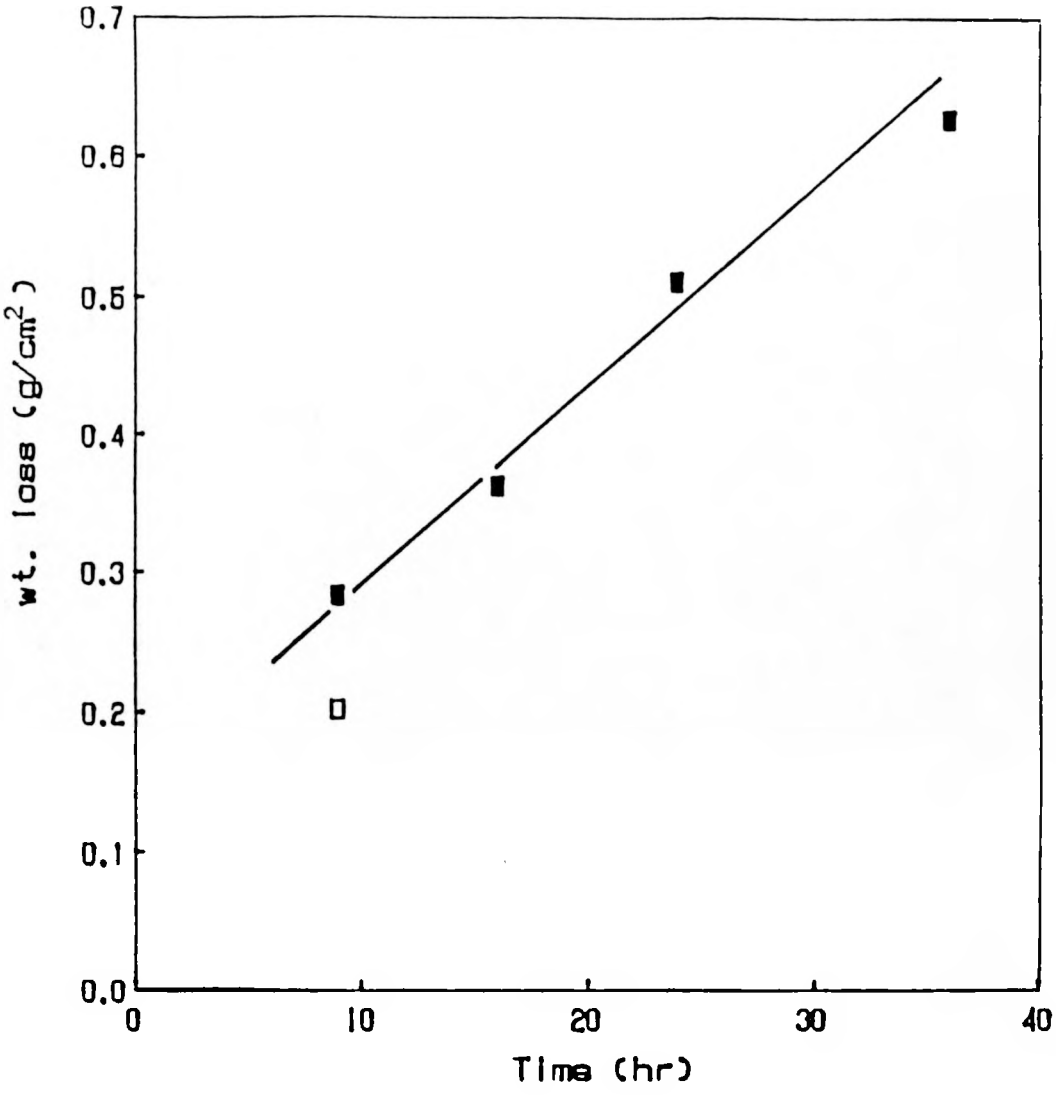

Figure 3. Metal wastage expressed as weight loss versus oxidation time at 1150°C with CO/CO_2=0.59. ■-unplated and □-plated 9Cr-1Mo alloy.

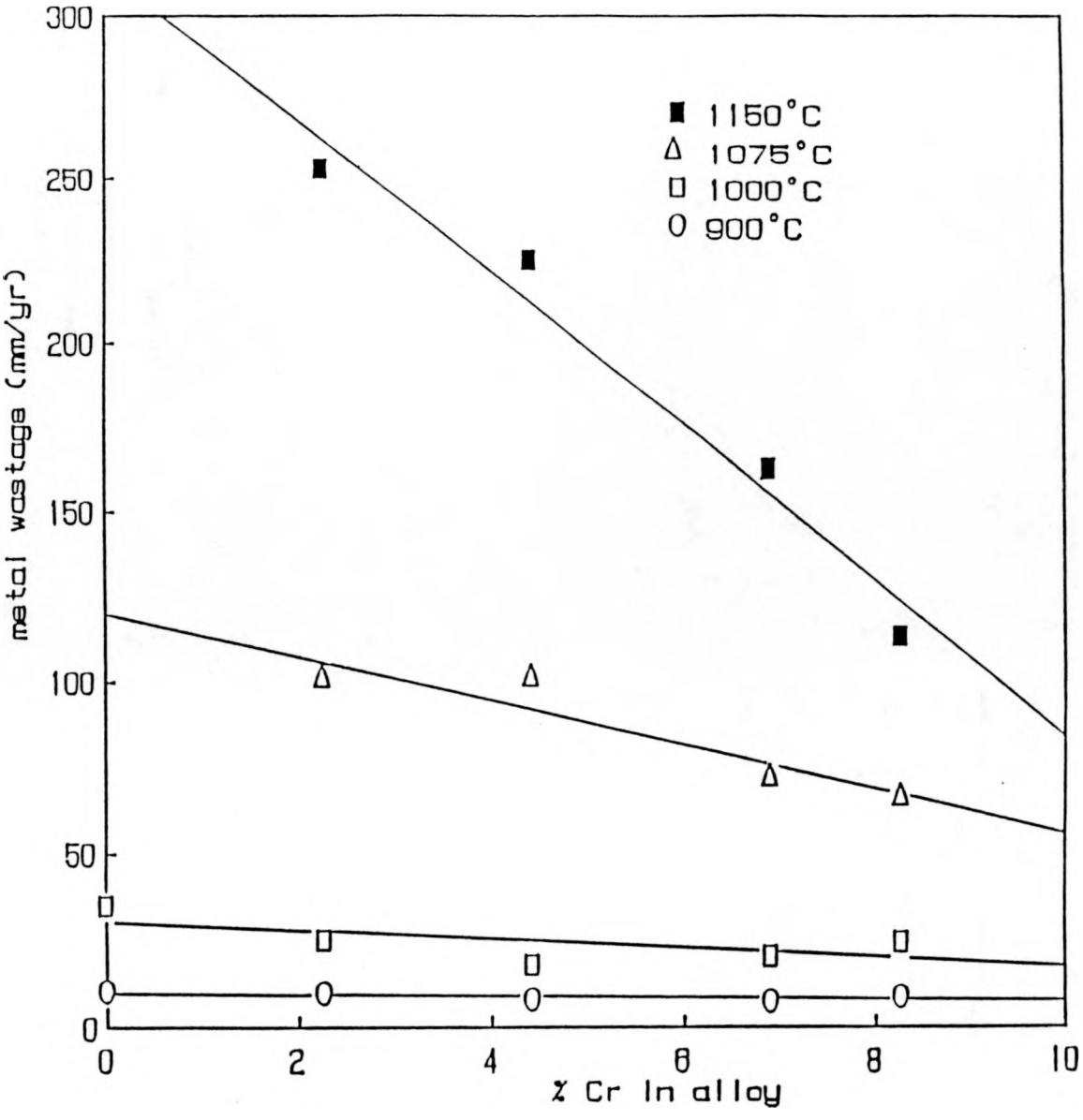

Figure 4. Metal wastage versus %Cr in Cr-Mo steels oxidized for 48 hr at 1150°C with CO/CO_2= 0.59.

increases with temperature and decreases with %Cr in the alloy. In this gas mixture, the beneficial effect of Cr increases with temperature, an effect which is believed to be due to the formation of a more protective inner layer of Cr-rich spinel at the higher temperatures. In all of the specimens except unalloyed iron, the outer layer of FeO had a tendency to spall.

Figure 5 shows a drawing of the microstructure of a 7 Cr-½Mo specimen after reacting for 32 hr at 1150°C with CO/CO_2 = 1.76. This microstructure is similar to the microstructures of the specimens whose oxidation rates are plotted in Figure 4 for a temperature of 1150°C. X-ray diffraction measurements clearly showed that the outer layer had the structure of FeO and that the inner layer had the structure of $(Fe, Cr)_3O_4$. In neither case was it possible to determine the relative amounts of Fe and Cr in the compounds. The particles in the internal oxidation zone were not identified, but are believed to be either spinel, or more likely, Cr_2O_3.

It was on the basis of this series of general oxidation experiments that it was decided to carry out defect healing experiments on specimens preoxidized for 16 hrs at 1150°C with CO/CO_2 = 1.76. These conditions produced a continuous, adherent spinel layer of an adequate thickness (approximately 25 micrometers).

Defect healing in sealed capsules: The details of the procedure used for these experiments was to preoxidize specimens at 1150°C for a sufficient time to obtain a spinel layer at least several micrometers in thickness. The FeO outer layer which had not spalled off was easily removed mechanically. Flaws were made on the surface, as depicted in Figure 6(a). The specimens were then sealed in evacuated Vycor glass capsules. With this procedure, the specimens could be reheated with virtually no oxygen present, except for that in oxide layers adjacent to the flaws. As shown in Figure 6(b), during reheating or healing, lateral mass transport of oxide into the flaws occurred. The thickness, composition, and structure of the oxide formed at the bases of the flaws were the parameters studied.

The experimental conditions and oxide compositions for several of these experiments are listed in Table 2. In the first two entries, data are given for the 7 and 9% Cr alloys. The important result for these specimens is that the Cr content of the oxide in the healed flaw was only about half that in the oxide adjacent to the flaw. It is believed that this effect is due to slower lateral diffusion of Cr into the flaw. Hodge (16) measured diffusion coefficients of Cr and Fe in spinel using radioactive tracers. The diffusion coefficients varied with oxygen partial pressure, but D_{Cr} was always 10^3 times slower than D_{Fe} at 1200°C. Since the ionic radii of Cr and Fe are nearly equal, the difference in diffusivities cannot be explained by a size effect. The explanation given by Hodge was that Cr exists as Cr^{3+}, while Fe is present predominately as Fe^{2+}. The difference leads to coulombic interactions which result in a lower jump frequency for Cr^{3+}.

It is useful to compare D_{Fe} in the spinel with D_{Fe} in FeO. From the data of Himmel et. al (17) for FeO, the comparison shows that Fe diffuses 150 or more times faster in FeO than in the spinel at 1200°C. Thus, the formation of an adherent spinel layer can be expected to result in relatively slow rates of both general oxidation and flaw healing by lateral diffusion.

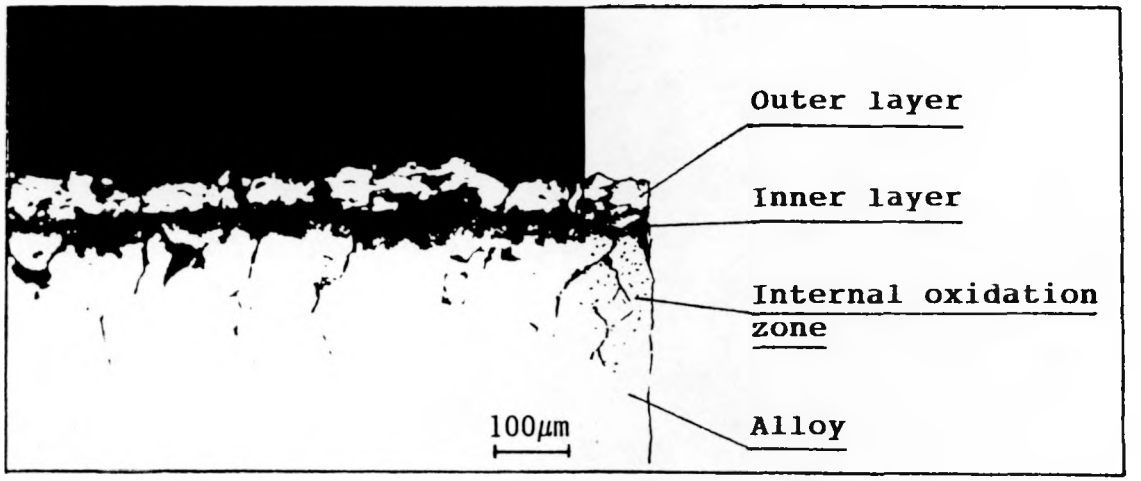

Figure 5. Cross section of 7Cr-½Mo steel specimen after oxidizing for 32 hours at 1150°C with CO/CO_2=1.76.

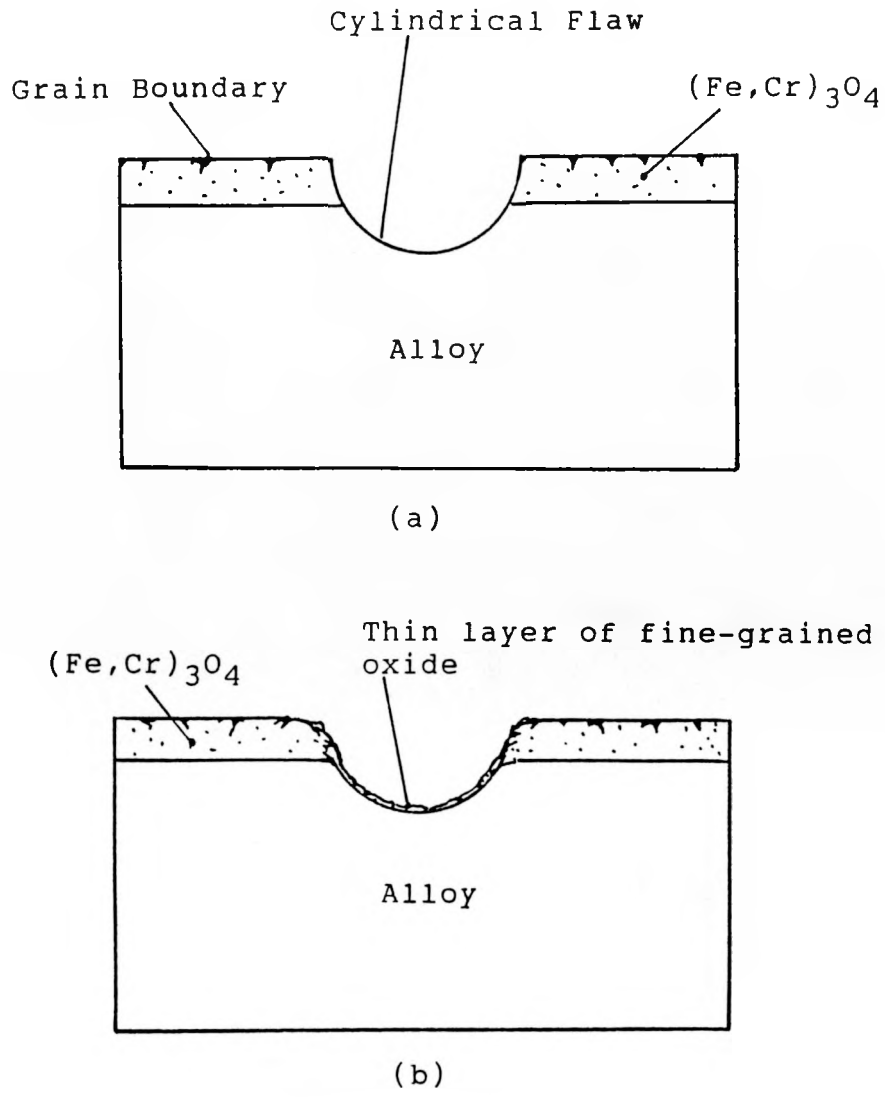

Figure 6. (a) Cylindrical flaw made with wire saw in preoxidized Cr-Mo steel specimens. (b) Spreading of oxide into flaw during thermal anneal in static vacuum.

Table 2 Oxide Composition in Flaws Healed in Static Vacuum

Alloy Designation	Preoxidation Conditions			Healing Conditions		Oxide Composition *	
	Temp (°C)	Time (hr)	Atmosphere	Temp (°C)	Time (hr)	Outside Flaw	Inside Flaw
7Cr-½Mo steel	1150	16	CO/CO_2=1.76	900	160	39Cr,59Fe 0.3Mo,1Al 1Si	20Cr,75Fe 1Mo,1Al, 3Si
9Cr-1Mo steel	1150	16	CO/CO_2=1.76	900	160	50Cr,49Fe 1Si	27Cr,47Fe 19Si,7Al
9Cr-1Mo steel (Cr-plated)	1150	16	CO/CO_2=1.76	900	160	16Cr,83Fe 0.3Mo,1Si	21Cr,78Fe 0.7Mo,1Si
Fe-25Cr-6Al	1150	16	CO/CO_2=1.76	900	160	10Cr,19Fe 69Al	24Cr,31Fe 32Al
Fe-25Cr-6Al	1150	48	Air	900	116	12Cr,6Fe, 83Al	27Cr,31Fe 42Al

* Basis: Weight percent metal, normalized to total metal content

Scanning electron micrographs of the 7Cr - ½Mo specimen are shown in Figure 7. The structure of the oxide at the base of the flaw shown in Figure 7(b) is finer than for the oxide outside the flaw shown in Figure 7(a). Within the flaw, individual grains of oxide were not resolvable, but some of the surface roughness from the wire saw was still evident in the oxide.

The same 7Cr-½Mo specimen was characterized by Auger electron spectroscopy (AES). The results of depth profile measurements in the flaw area are shown in Figure 8. The Cr concentration appears to be between 5 and 10 atomic percent and changes only slightly with distance from the surface. However, analysis for Cr in steels by AES is not very accurate because of overlapping Cr and O spectra. In examining the Fe and O concentrations for sputtering times up to 47 minutes, it appears that the oxide is non-stoichiometric, with the Fe-O ratio increasing with depth. From the sputter rate, the oxide layer in the flaw is approximately 2000A (0.2 microns) thick. For longer sputtering times, it is likely that the beam is penetrating into the metal phase and is touching some oxide particles formed by internal oxidation. The AES results are generally consistent with the EDX results listed in Table 2 because both show a depletion of Cr in the oxide formed in the flaw.

The third entry in Table 2 gives results for a Cr-plated 9Cr-1Mo specimen. Scanning electron micrographs for the same specimen are presented in Figure 9. The EDX data show that the Cr content of the oxide inside the flaw was higher than in the adjacent scale (20.5 vs 15.8%). In all of the other examples discussed, the reverse was true; there was a depletion rather than an enrichment of Cr inside the flaw. The enrichment found for the Cr-plated specimen is believed to be due to one or more of the following effects:

(a) FeO formed during preoxidation did not spall off and contributed to the low Cr concentration adjacent to the flaw. Oxide formed within the flaw was predominately or entirely spinel.

(b) The flaw was cut into alloy material with a relatively high Cr concentration. During the healing treatment, Cr below the base of the flaw could have diffused to the surface and scavenged oxygen from the FeO phase adjacent to the flaw, thereby enriching the healed oxide in Cr.

(c) The flaw was cut into material which contained particles of Cr_2O_3 or spinel formed by internal oxidation. These oxide particles would influence both the amount and composition of oxide layer shown in Figure 9(b).

This enrichment of the healed oxide in Cr is potentially important. The reason is that it could be more protective against further oxidation to the underlying alloy. More effort would be needed to obtain a clear understanding of the mechanism of enrichment and its practical implications.

The last two entries in Table 2 give results for Fe-25Cr-6Al specimens preoxidized and healed under different conditions. In both cases, there was a significant depletion of aluminum oxide in the flaw area. This result parallels the results for unplated Cr-Mo steels, in that slow lateral diffusion of one of the species, Al ions in this case, was probably responsible for the depletion effect. Because of the Al depletion, there is a corresponding

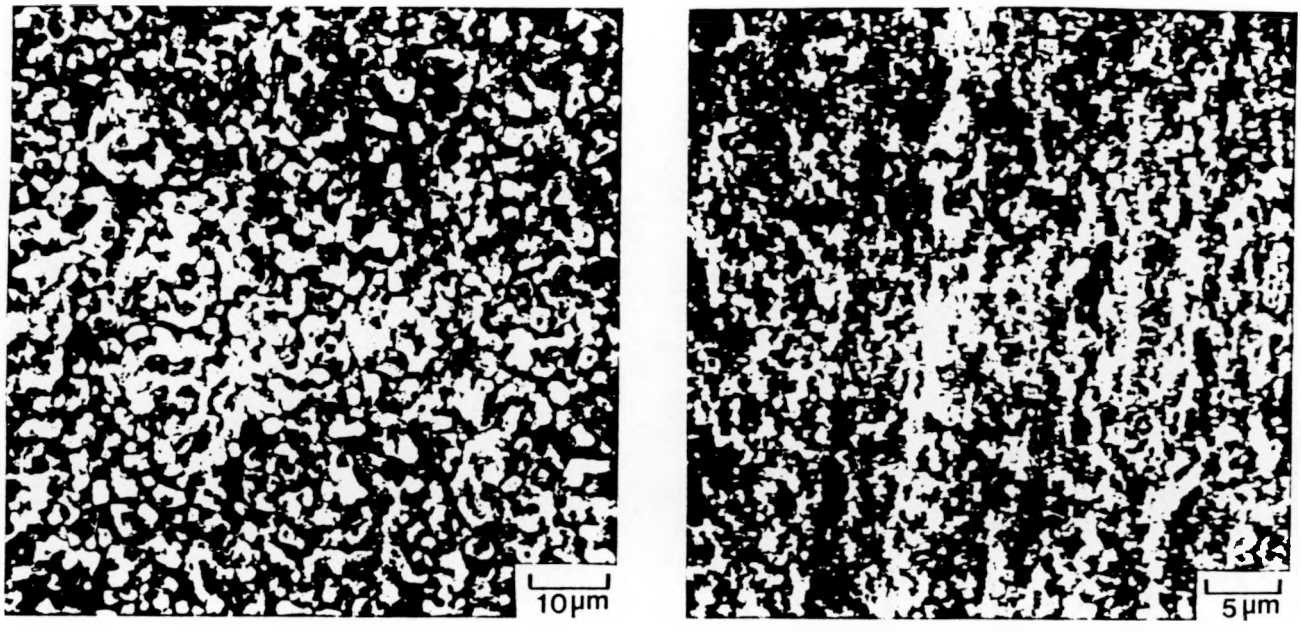

(a) (b)

Figure 7. Scanning electron micrographs of 7Cr-½Mo alloy after thermal healing of oxide at 900°C in static vacuum: (a) outside the flaw (b) inside the flaw.

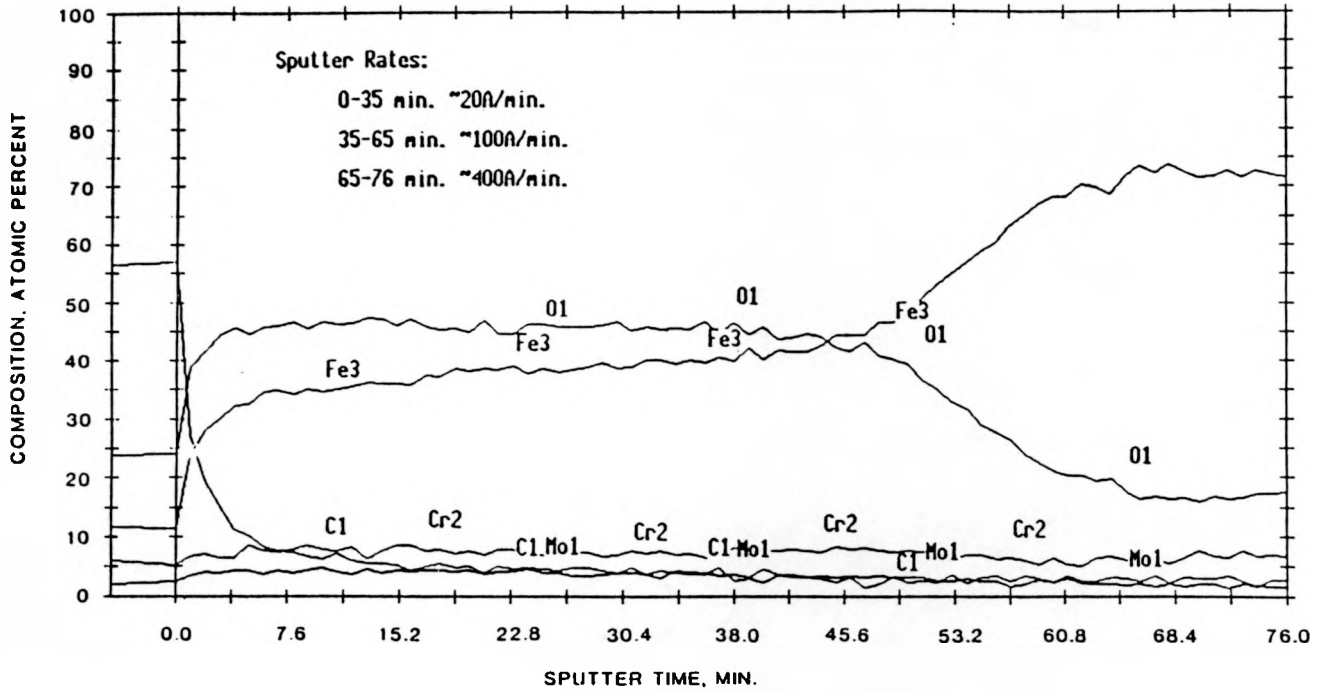

Figure 8. Auger depth profile data for oxide at base of healed flaw in 7Cr-½Mo steel specimen shown in Fig. 7.

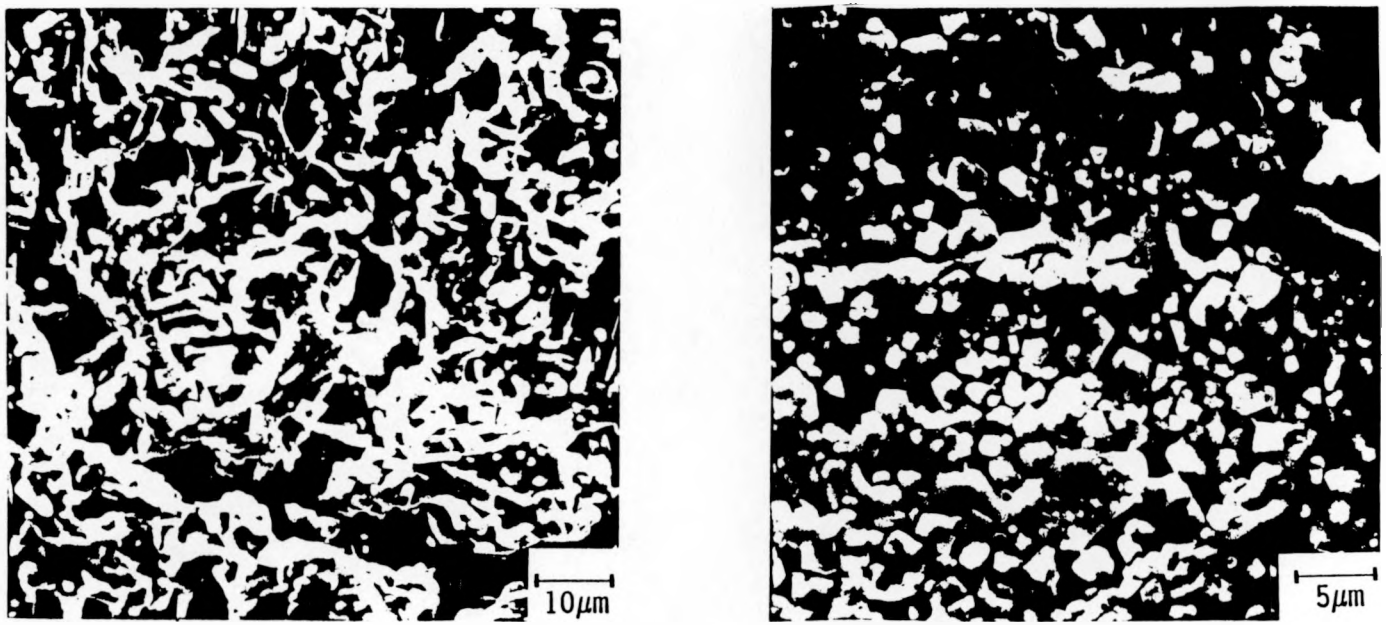

(a) (b)

Figure 9. Scanning electron micrographs of Cr-plated, 9Cr-1Mo alloy after thermal healing of oxide at 900°C in static vacuum: (a) outside the flaw (b) inside the flaw.

enrichment of chromium oxide inside the flaws, which could give a protective character to the oxide layer formed during healing.

Healing in oxidizing atmosphere: In this series of experiments, the specimens were preoxided and flaws made in the same manner as described above. Healing treatments, however, were carried out in the same gas atmosphere as used for preoxidation. Experiments of this type simulate more closely service conditions for the material, but there is a drawback in that it is more difficult to distinguish between lateral mass transport of oxide into the flaw and new oxide formed by reaction with gaseous species. Changes in the dimensions of the flaws were used as the principal criterion for separating the two effects.

Figure 10 shows the cross-section of a flaw in a 9Cr-1Mo alloy specimen after healing for 24 hr at 900°C. A gas mixture with CO/CO_2 = 1.76 was used for both preoxidation and healing. The characteristics of the flaw after healing show no clear evidence that lateral mass transport was significant. There was no appreciable shallowing, and the zone of internal oxidation progressed deeper into the specimen, as one would expect if direct oxidation occurred at the base of the flaw.

Figure 11 shows the cross-section of another 9Cr-1Mo alloy specimen healed for 3 hr at 1150°C in the same atmosphere. Although not dramatic, there was some evidence for lateral mass transport at the higher temperature. This conclusion is based on the development of thicker layers of both oxides at the top edge combared to the base of the flaw.

Additional experiments of this type were carried out on the Fe-25Cr-6Al alloy. The top view of one of the specimens is shown in Figure 12. The specimen was preoxidized for 48 hr in air at 1150°C, and the defect healing treatment was the same. Parts (a) and (b) show the same flaw before and after the healing treatment. There was no measurable shallowing or narrowing of the flaw during healing. EDX measurements gave approximately 80% Al both inside and adjacent to the flaw. Thus the normal protective oxide scale reformed in the flaw by direct oxidation during the healing treatment.

It was possible to show a marked difference between healing of the oxidation-resistant alloys discussed above with unalloyed iron. Figure 13 shows a pair of scanning electron micrographs of a specimen preoxidized for 16 hr at 1150°C with CO/CO_2 = 1.76, then healed for 4½ hr under the same conditions. In part (a), a flaw is shown before healing. In part (b), the same flaw virtually disappeared during the healing treatment. The FeO grains are smaller where the two sides of the flaw grew together, but there was no indentation of the surface. Without doubt, lateral mass transport was the dominant effect because of high diffusion rates in FeO.

Healing with noble metal simulated defects. The final set of experiments consisted of observing the extent to which an oxide scale will grow laterally over a platinum band embedded in the surface of a specimen. Specimens for these experiments were prepared by cutting grooves in the unoxidized surface with a wire saw. Then platinum wires were pressed into the grooves and diffusion bonded to the specimen by heat-treating in an H_2 atmosphere at 1150°C. Finally the surface was polished to remove excess platinum.

Figure 10. Scanning electron micrograph of flaw in 9Cr-1Mo alloy after healing for 24 hours at 900°C in gas mixture with CO/CO_2=1.76.

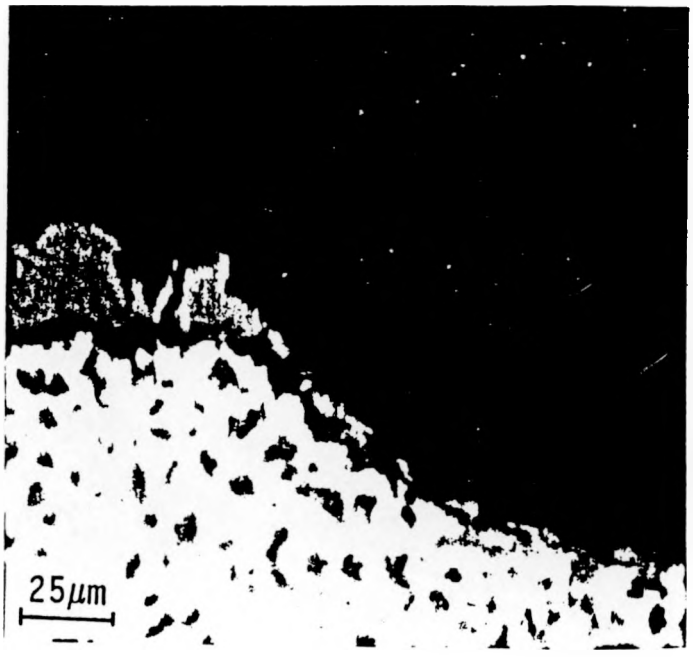

Figure 11. Photomicrograph of edge of flaw in 9Cr-1Mo alloy after healing for 3 hours at 1150°C in gas mixture with CO/CO_2=1.76.

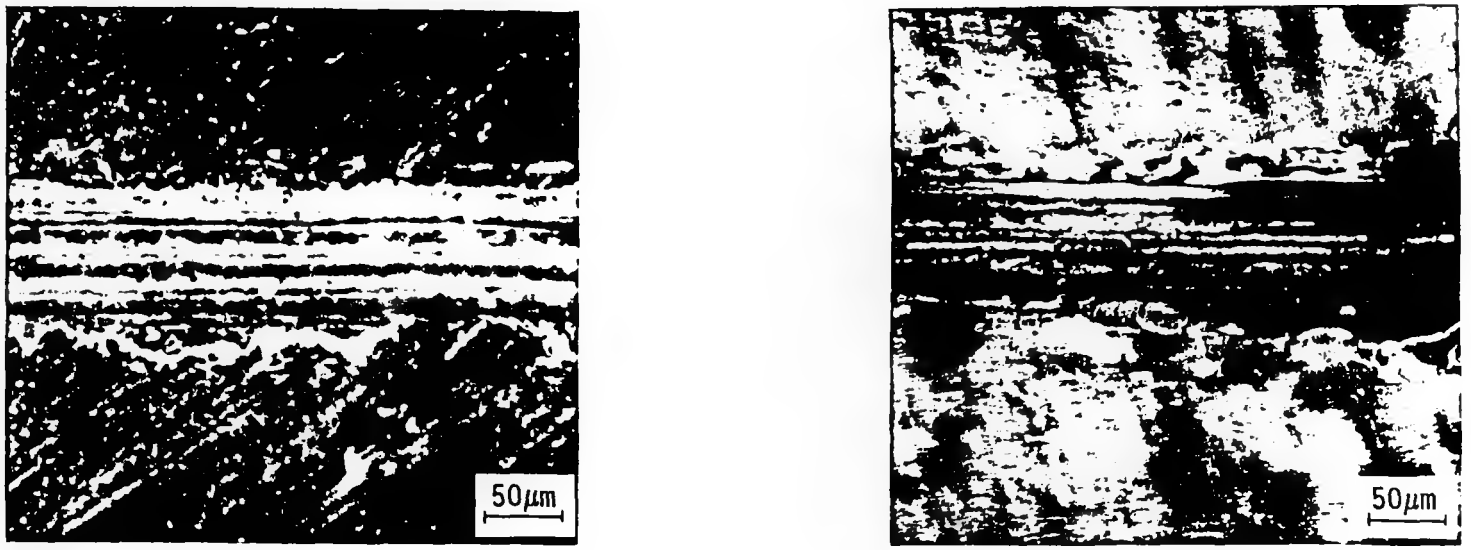

(a) (b)

Figure 12. Thermal healing of oxide on Fe-25Cr-6Al alloy: (a) Appearance of flaw made after preoxidation for 48 hr at 1150°C in air. (b) appearance of same flaw after healing under same conditions.

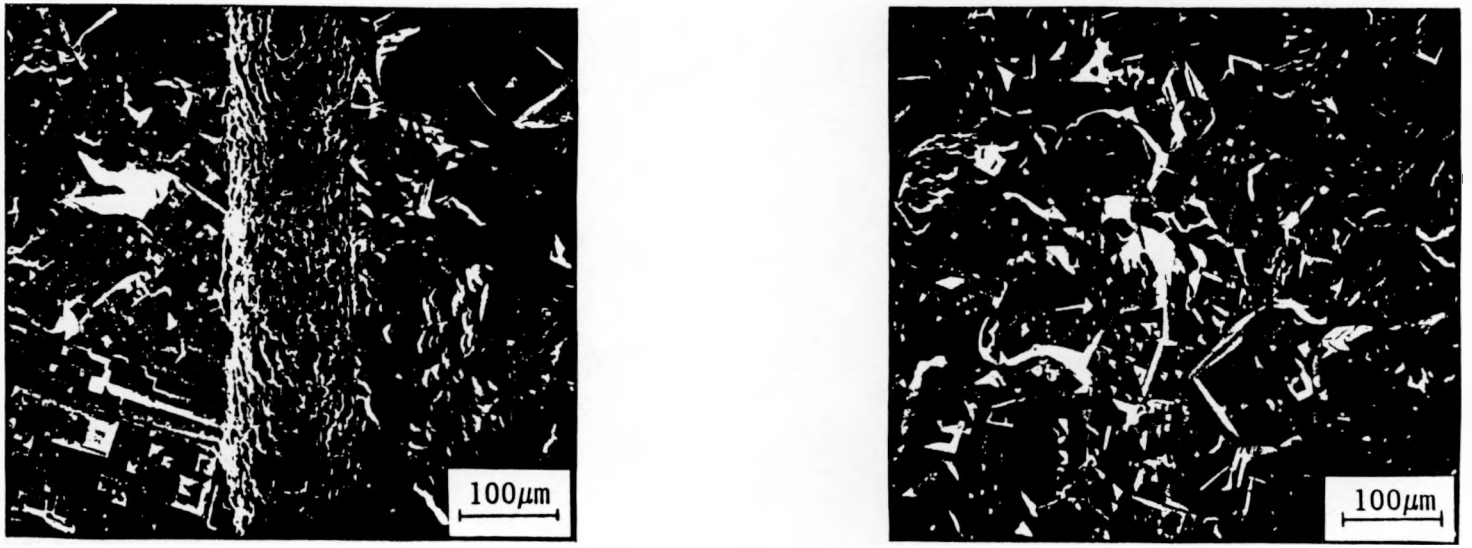

(a) (b)

Figure 13. Thermal healing of oxide on unalloyed iron specimen: (a) appearance of flaw made after preoxidation for 16 hr at 1150°C with CO/CO=1.76 (b) appearance of same flaw after healing for 4½ hr at 1150°C in same atmosphere.

The specimens were oxidized under various conditions to study the tendency of oxide formed on the alloy surface to extend over the Pt simulated defect. Since Pt and other metals have a higher surface free energy than oxide scales, there is a thermodynamic driving force for the oxide to cover the exposed metal, as was the case for flaws cut through the scales to expose bare metal at the base of the flaws in the experiments described earlier.

The results of one of these experiments is shown in Figure 14. The 9Cr-1Mo alloy was oxidized for 6 hr at 1150°C in a gas mixture with CO/CO_2 = 1.76. Immediately after removal from the furnace, it was observed that a loosely adherent scale, presumed to be FeO, completely covered the Pt band. Figure 14 shows the appearance after removal of the loose scale. At first, it was thought that a spinel layer had begun to grow over the Pt band also because the Pt band was narrower than before oxidation. However, Auger and EDX measurements on the portion of the sample adjacent to the exposed Pt proved that a Pt-Fe alloy or intermetallic layer had formed by diffusion.

Additional experiments of this type were carried out on the 9Cr-1Mo alloy at 900°C, and on the Fe-25Cr-6Al alloy at 1150 and 900°C. In none of these experiments was there a significant amount of oxide growth over the platinum. These results contrast with results published on unalloyed iron(12), where FeO layers grew over gold bands rather rapidly at 720°C.

General discussion. When the results for all three types of experiments are considered, a consistent picture emerges. If FeO (probably containing Cr) forms in the scale, lateral mass transport of the FeO into simulated defects occurs at an appreciable rate. This behavior is explainable in terms of the high diffusion coefficient of Fe^{2+} in FeO. If spinel of the type $(Fe,Cr)_3O_4$ or Al-rich oxide forms in the scale, lateral mass transport of these species is much slower because of the lower diffusion coefficients. The manner in which flaw healing occurs by lateral mass transport in the alloys studied is unfortunate because FeO would not provide much protection against further oxidation while the spinel and Al-rich oxides would.

The experiments conducted on the 9Cr-1Mo alloy surface-modified by Cr plating gave encouraging results which should be pursued. The results were encouraging in that a Cr enrichment was obtained in healed flaws compared to the scale adjacent to the flaws. Otherwise, if improvements are to be made in flaw healing behavior, consideration should be given to studying new alloy compositions which strike a balance between flaw healing characteristics and general oxidation rates.

CONCLUSIONS

(1) In $CO-CO_2$ gas mixtures, the beneficial effect of Cr in Cr-Mo steels is much greater at 1150°C than at 900°C.

(2) Enriching the surface of 9Cr-1Mo steel with electroplated Cr has a beneficial effect on both the general oxidation rate and flaw healing behavior.

(3) In flaw healing experiments, lateral mass transport of FeO in scales was much greater than for Fe-Cr spinel and Al-rich oxide phases.

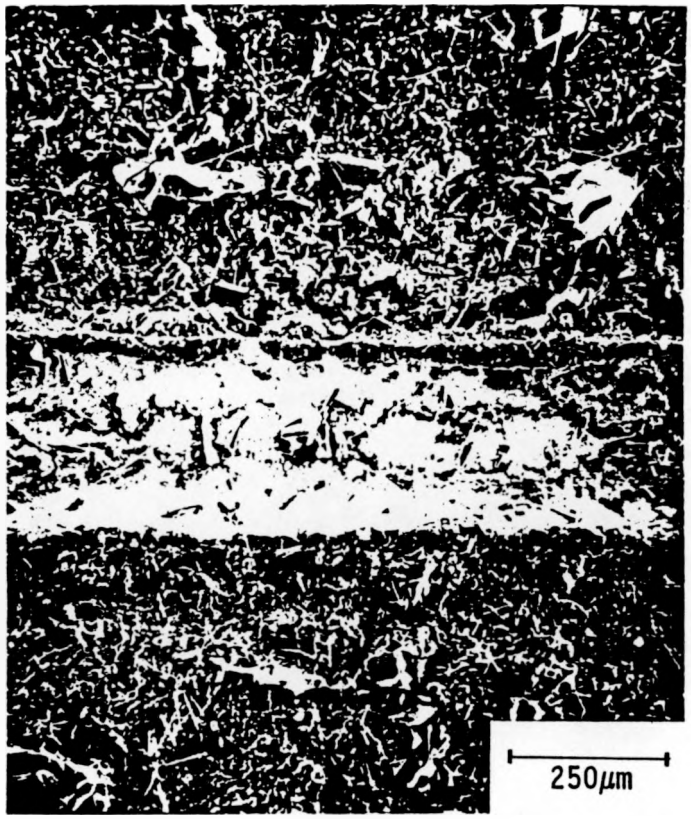

Figure 14. Scanning electron micrograph showing surface of a 9Cr-1Mo alloy specimen containing a Pt band after oxidation at 1150°C for 6 hr with CO/CO_2=1.76 and removal of non-adherent oxide.

(4) Examining new alloy compositions could result in a better compromise between general oxidation resistance and flaw healing characteristics.

ACKNOWLEDGMENT

Financial support for this project was provided by the U.S. Department of Energy under Contract No. DE-FC22-89PC89904.

REFERENCES

1. K. Hauffe, Oxidation of Metals, Plenum Press, New York (1965).

2. D.S. Douglass, ed., Oxidation of Metals and Alloys, American Society for Metals, Metals Park, OH (1971).

3. N. Birks and G.H. Meier, Introduction to High Temperature Oxidation of Metals, Edward Arnold Press, London (1983).

4. D.B. Meadowcroft and M.I. Manning, eds., Corrosion Resistant Materials for Coal Conversion Systems, Elsevier Applied Science Publishers, New York (1984).

5. J.F. Norton, ed., High Temperature Materials Corrosion in Coal Gasification Atmospheres, Elsevier Applied Science Publishers, New York (1984).

6. M.G. Rothman, ed., High Temperature Corrosion in Energy Systems, Amer. Inst. of Mining, Metallurgical and Petroleum Engineers, New York (1985).

7. P.L. Harrison, R.B. Dooley, S.K. Lister, D.B. Meadowcroft, P.J. Nolan, R.E. Pendlebury, P.L. Surman, and M.R. Wootton, "The Oxidation of 9Cr 1Mo Steels in Carbon Dioxide, a Discussion of Possible Mechanisms," Proceedings of International Conference on Corrosion of Steels in CO_2, D.R. Holmes, R.B. Hill, and L.M. Wyatt, Ed., British Nuclear Energy Society, 1974, pp. 220-233.

8. M.G.C. Cox, B. McEnaney, and V.D. Scott, "Structure and Growth of Oxide on Iron-Chromium Alloys," Ibid., pp. 247-256.

9. P.L. Surman, J. Bettelheim, R.B. Dooley, J. Graham, D.B. Meadowcroft, and P.C. Rowlands, "Methods of Controlling the Oxidation of 9Cr/1Mo Steel in High Temperature CO_2," Ibid., pp. 257-271.

10. M. Schutz, "The Healing Behavior of Protective Oxide Scales on Heat-Resistant Steels after Cracking under Tensile Strain," Oxidation of Metals, vol. 8, (1986), pp. 409-421.

11. V. Srinivasan and K. Vedula, ed., Corrosion and Particle Erosion at High Temperatures, The Minerals, Metals and Materials Soc., Warrendale, PA, 1989.

12. J.H. Swisher, W.D. Cho, and S.C. Chang, "Thermal Healing of Defects in Wustite Films on Iron," op. cite., pp. 547-564.

13. J. Crank, The Mathematics of Diffusion, Oxford Univ. Press, Oxford UK, 1967, pp. 9-11.

14. J.F. Elliott, M. Gleiser, and V. Ramakrishna, Thermochemistry for Steelmaking, vol. 2, Addison-Wesley Publ. Co., Reading, MA, 1963, p. 691.

15. F.S. Pettit, R. Yinger, and J.B. Wagner, "The Mechanism of Oxidation of Iron in Carbon Monoxide-Carbon Dioxide Mixtures," Acta Met., vol. 8, 1960, p. 617.

16. J.D. Hodge, "Diffusion of Chromium in Magnetite as a Function of Oxygen Partial Pressure," J. Electrochem. Soc., vol. 125, no. 2, 1978, pp. 55C-57C.

17. L. Himmel, R.F. Mehl, and C.E. Birchenall, "Self-Diffusion of Iron in Iron Oxides and the Wagner Theory of Oxidation," J. Metals, vol. 5, 1953, pp. 827-843.